Desalination and Water Treatment
www.deswater.com

doi: 10.5004/dwt.2022.28504

262 (2022) 312–322
June

Green synthesis of TiO_2 using *Ocimum basilicum* leaf extract and its application in photocatalytic degradation of amoxicillin residues from aqueous solution

Fadia A. Sulaiman[a], Abeer I. Alwared[b,*]

[a]*Water Resource Technical, Al-Hawija Technical Institute, Bahgdad, Iraq, email: fadiah_hwj@ntu.edu.iq*
[b]*Department of Environmental Engineering, College of Engineering, University of Baghdad, Iraq, email: dr.abeer.wared@coeng.uobaghdad.edu.iq*

Received 30 December 2021; Accepted 9 April 2022

ABSTRACT

Much research has been triggered by interest in green synthesis because it is low in toxicity and high in reproducibility, as well as pollution-free and cost-effective. The aim of this study is the production of titanium dioxide nanoparticles using basil leaf (B-TiO_2). The formation, size, and shape of the B-TiO_2 particles were confirmed via spectroscopy and microscopy using the X-ray diffraction, Fourier-transform infrared spectroscopy, and scanning electron microscopy techniques to investigate the B-TiO_2 synthesized. The photocatalytic effectiveness of the B-TiO_2 nanoparticles was examined by degrading the amoxicillin (AMOX) residue from an aqueous solution using solar irradiation. From the findings the B-TiO_2 was proven to be highly capable of treating AMOX-contaminated water and showed maximum removal efficiency, achieving 91.36% under the best operational conditions of pH 5, and specific concentrations of B-TiO_2 (25 mg/L), H_2O_2 (500 mg/L) and AMOX (10 mg/L). Besides, the results showed that during the decomposition process the elimination of total organic carbon achieved 86.24% and intermediate compounds were generated when GC-Mass testing was done. In the present study, it was confirmed that during the degradation of AMOX the green synthesis of the B-TiO_2 photocatalyst nanocomposite, in a solar–photocatalytic reactor, at optimum operating conditions, revealed acceptable efficiency.

Keywords: Synthesis; TiO_2; Basil leaves; Amoxicillin residues; Advanced oxidation processes; Solar irradiation

1. Introduction

The presence of antibiotics in wastewater continues to pose an increasing and alarming threat to environmental and human health, encouraging the advancement of bacterial resistance to antimicrobials [1]. Among the many medicinal substances, antibiotics have attracted special attention. Due to their active reactions even in very low concentrations, they have grown into a huge hazard as they are a real threat to the health of humans as well as the environment [2]. Besides they play a potential part in the production of antibiotic-resistant bacteria [3]. Antibiotics are present in the wastewater discharged into the environment from industries (pharmaceutical), hospitals, households, and livestock. Also, as approximately only 30% of the antibiotics consumed by humans and animals diffuse through the body systems to combat disease, the rest of the 70% enters the environment through defecation, without undergoing metabolization [4].

Considering the water treatment technologies in use thus far, the advanced oxidation processes (AOP) involve technologies that release hydroxyl radicals, following which the organics are completely mineralized into water and CO_2 without the generation of any unsafe or harmful by-products [5]. Different catalyst has been used in AOP, TiO_2 nanoparticle is the most widely used semiconductor for

* Corresponding author.

their many beneficial properties, namely, it is cost-effective, low in toxicity, chemically stable, as well as possesses a broad bandgap and high photosensitivity in the presence of oxygen. [6]. Different chemical and physical methods have been used in the synthesis of TiO_2, which are harmful to the environment and human health. However, the stability of the catalyst, which is related to its capability of being reused, is an important aspect for industrial or commercial applications. Despite the existence of commercial catalysts with excellent photocatalytic efficiency, full-scale, heterogeneous, photocatalysis systems are still rare due to the aggregation during the operation and difficult recovery and reuse after the process [7]. To overcome these problems different techniques have been used by researchers such as adding different compounds such as diverse biopolymers and carbon materials [8], graphene oxide–chitosan hydrogel [9]; GO/TiO_2 nanocomposite, and GO nanosheet [10], and/or using a new technique for synthesizing nontoxic nanoparticles. The biological synthesis of nanoparticles is a one-step bioreduction approach that uses less energy and is environmentally friendly. Among the different methods used in the synthesis of nanoparticles titanium dioxide, the biosynthetic process (also denoted as obtained from plants and microorganisms [11]. The green synthesis of nanoparticles is superior as it is a single-step technique, which is cost-effective, eco-friendly, and pollution-free, besides involving a low consumption of time and energy and providing a high yield of homogeneously composed particles [12]. A variety of materials have been used by many researchers including *Zizyphus spina-christi* leaves [13]; piper betel, *Ocimum tenuiflorum*, *Moringa oleifera*, and *Coriandrum stadium* for the extract in the green synthesis of nano TiO_2 [14]; *Moringa oleifera* [15]; *Curcuma longa* aqueous extract [11]; *Aloe vera* [16]; *Azadirachta indica* [17]; *Catharanthus roseus* [18]; and nyctanthes leaves [19].

Although UV light possessing high energy has shown great effectiveness in the removal of pollutants, the development of UV-industrialization is limited because of the following reasons. (1) UV light sources are relatively expensive, unstable, and energy-consuming. (2) The proportion of UV light in sunlight irradiated to the Earth's surface is less than 5%, and using UV light as a light source cannot make full use of solar energy. Therefore, in order to utilize solar energy as a green energy source, more researchers have recently turned their attention to visible light, simulated sunlight, and even real sunlight [20]. For that, solar-light-driven advanced oxidation processes (AOPs) are renewable and green environmental restoration.

Although there are studies evaluating the removal of the antibiotic amoxicillin (AMOX) from aqueous solutions and there are studies on the synthesis of nanoparticles from plants such as basil, there is no study that combined the two. Therefore, it would be interesting to investigate the conditions for the removal of the antibiotic amoxicillin (AMOX) from solutions aqueous using TiO_2 nanoparticles extracted from the basil plant, For that the present study involved the production of a novel, eco-friendly, inexpensive, and sustainable synthesis of the TiO_2 nanoparticles extracted from the plant *Ocimum basilicum* (basil) plant. Besides, it also examined the effectiveness of green synthesis TiO_2 nanoparticles for the removal of AMOX antibiotics from aqueous solutions by employing a solar photocatalytic reactor and investigating the various parameters of pH, time, and the concentrations of TiO_2 and AMOX.

2. Materials and methods

2.1. Materials

In this model, the contaminant selected was powdered amoxicillin (AMOX) of 99% purity, with no need for further purification, procured from the General Company for Drugs Industry (Iraq) (original manufacturer: Merck, Germany). Table 1 reveals their chemical structure and specifications, respectively. The Titanium Tetra-Isopropoxide (TTIP) was composed of 95% anatase and 5% rutile. Isopropanol. Hydrogen peroxide H_2O_2 (50% w/w) was purchased from Merck. Either HCl and/or NaOH was used to adjust the pH value of the aqueous solution. Preparation of the nanostructured titanium oxide was done using fresh basil leaves.

2.2. Methods

2.2.1. Green TiO_2 nanoparticles

First, the fresh basil leaves were gathered, thoroughly washed in tap water and then rinsed with distilled water. They were heated next for 2 h in 125 mL of distilled water at 70°C. The solution extract was filtered and stored for later use. Next, 250 mL of the extracted solution was taken, to which 10 mL of Titanium tetra-isopropoxide (TTIP) was added in a dropwise fashion. This was then placed on a stirrer for 4 h, at 980 rpm and then set aside for a whole night to stand and cool down to room temperature. The solution was then filtered and oven-dried under hot air at 70°C for 12 h. After the nanoparticles were collected, they were subjected to calcination at 400°C for 2 h in a muffle furnace. These calcinated nanoparticles, termed B-TiO_2 nanoparticles, were removed and stored for later use [12].

2.2.2. Procedure and analysis

The process of photocatalytic degradation was performed in a batch mode reactor using solar irradiation, Fig. 1. The reactor was made of Pyrex glass (1L), with reflective power for solar irradiation [22], using a piece of mirror placed at the bottom (used as a reflector). Next, different concentrations of AMOX solution (10, 25, 50, 75, and 100) mg/L were prepared and adjustments were made to the pH, (employing a pH meter model INOLAB

Table 1
Amoxicillin properties

Parameter	Character/value
Molecular formula	$C_{16}H_{19}N_3O_5S$
Molar mass	365.4 g/mol
Solubility in water	3,430 mg/L at 20°C
Dissociation constant (pKa)	2.4 (carboxyl), 7.4 (amine), and 9.6 (phenol)
Henry's law constant	2.73×10^{-19} at 20°C

Source: Balarak et al. [21]

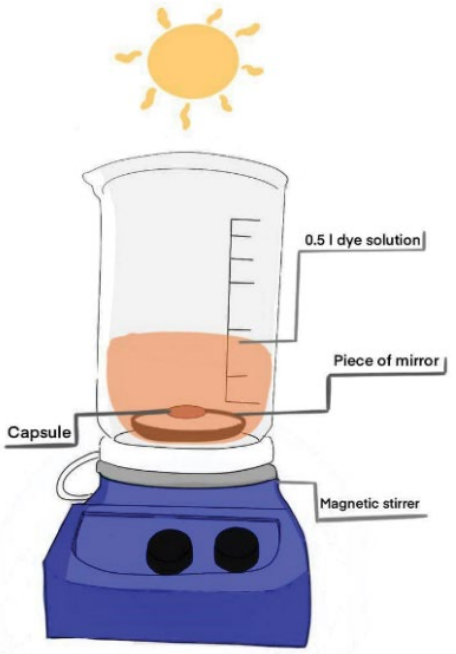

Fig. 1. Schematic of photo-oxidation process using solar source.

72, WTW Co., Weilheim, Germany) by using dilute HCl or NaOH solution to the contents of the reactor. Once this was accomplished, the intended concentrations of the B-TiO_2 nanoparticles 25, 75, and 150 mg/L were poured into the solution. The suspension was placed on a magnetic stirrer (model MSH-300N, BOECO, Hamburg, Germany) at 200 rpm for 150 min. The primary adsorption equilibrium was achieved between AMOX and TiO_2, by leaving the solution in the dark for 30 min; the next step was the addition of H_2O_2 250, 500, and 750 mg/L and the lamp was switched on to kick-start the reaction. At particular time intervals, 10 mL of the sample was drawn out. It was centrifuged at 200 rpm for 15 min until the catalyst separated out. The concentration of AMOX in each sample was quantified using a spectrophotometer (UV-Vis Spectrophotometer Perkin-Elmer 55 OSE) at a maximum of 278 nm. However, calculation of the removal efficiency of the target compounds was done applying the equation given below:

$$\text{Removal percentage} = \frac{C_o - C_e}{C_o} \times 100 \quad (1)$$

where C_o and C_e refer to the concentrations of the primary and equilibrium drug (mg/L), respectively.

3. Results and discussion

3.1. Characteristic of B-TiO_2

The variations and similarities between the characteristic features of the commercial TiO_2 nanoparticles and B-TiO_2 nanoparticles (synthesized) were examined, using the Fourier-transform infrared spectroscopy (FTIR), scanning electron microscopy (SEM), and X-ray diffraction (XRD), and analyses were done.

3.1.1. Fourier-transform infrared spectroscopy

Employing the FTIR analysis the structure of the substance was determined. Also, the creation of the desired bonds, their nature and the active groups which constitute the catalyst surface were identified and verified through the analyses [23]. For the present study, the FTIR analyses of the B-TiO_2 and commercial TiO_2 were performed with the help of a JASCO 4100 device, in the 500–4,000 cm^{-1} spectral range, at the University of Tehran. The findings are shown in Fig. 2. The peaks observed from 500 to 800 cm^{-1} were most likely caused by the Ti–O stretching bands, linked to the creation of the TiO_2 nanoparticles, while the peaks at 1,631.48 and 1,636.33 cm^{-1} were attributed to the titanium carboxylate, which gave rise to the CH_3 stretching frequency peaks at 2,921 cm^{-1}, and the –OH group stretching and bending vibration maxima were seen at 3,423.99 and 1,631.48 cm^{-1}. The Ti–O–Ti stretching frequency was noted to peak at 1,395.25 cm^{-1}. The maxima of 800 and 1,395.25 cm^{-1} show some relationship [14]. From the FTIR spectrum, no substantial differences were identified between the green synthesis and commercial TiO_2. Further, when new ranges disappear or emerge, they are indicative of overlap between the AMOX and B-TiO_2 [24].

3.1.2. Scanning electron microscopy

The SEM enabled the study of the grain-size, shape and surface properties, such as morphology, for the commercial TiO_2 and B-TiO_2, prior to and post elimination of the AMOX residue from the aqueous solutions. This test was performed at the University of Tehran with the ZEISS model of this tool, Sigma V PEDS and mapping: Oxford instruments. The results of this investigation are shown in Fig. 3. Fig. 3a and b show that prior to the treatment, the morphology of both the B-TiO_2 and commercial TiO_2 possessed consistent but rough surfaces and had irregular spherical aggregates [25]. The presence of several cavities and tiny pores was also noted, a clear indicator of the suitability of the B-TiO_2 for photocatalytic applications [26]. However, Fig. 3c and d reveal significant changes in the morphological properties of both the commercial and B-TiO_2 which occurred during the antibiotic adsorption process. As the pore surfaces were completely filled up with the antibiotic particles, the catalyst surface revealed visible changes, becoming brighter and smoother, with the combination of some of the aggregates that had been separated earlier. The antibiotic adsorption was seen to occur on the active surface groups inside the pores, based on which the well-defined pores on the catalyst may provide the principal interpretation for the intense uptake of the antibiotic.

3.1.3. BET methods

The BET surface area and total pore volume for B-TiO_2 were 95.727 m^2/g and 0.2865 cm^3/g, respectively while that for commercial TiO_2 nanoparticles were 35.959 m^2/g and 0.072655 cm^3/g, respectively. This can be attributed to the porous structure of the green TiO_2 particles as well as their small particle size [27]. The larger surface area and pore volume provide a greater number of active sites on the surface

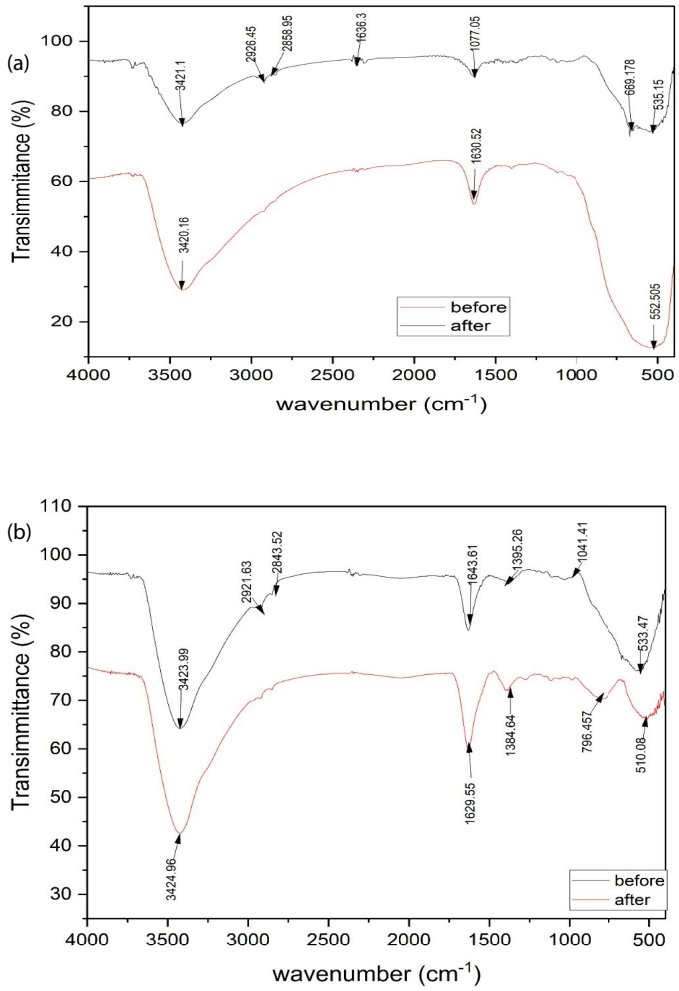

Fig. 2. FTIR analysis for commercial and B-TiO_2 before and after photocatalytic: (a) commercial TiO_2 and (b) B-TiO_2.

for further adsorption of reactive molecules, which results in a photocatalytic reaction with higher efficiency [28].

3.1.4. X-ray diffraction technique

The powder XRD method is one of the most effective scientific tools used to identify and quantify many types of crystalline materials with identical or closely similar chemical compositions but having a variety of crystal formations. From Fig. 4 the crystallization of the B-TiO_2 and commercial TiO_2 samples appeared almost similar, with the XRD pattern for the B-TiO_2 visible at an angle from $10° < 2\theta < 80°$. The tallest peaks are seen at about 25°, 38°, 48°, 55°, 63°, 70°, and 75°. Based on the pattern, the strong direction peaks at the values of 2θ are possibly caused by the structure of the B-TiO_2, whose hk_1 values of the exact B-TiO_2 peaks are linked to the 101, 004, 200, 211, 206, 213, and 215, respectively; for the commercial TiO_2, however, whose hk_1 values of the exact commercial TiO_2 peaks at the same value of 2θ are associated with 101, 004, 200, 211, 206, 213 and 215, respectively. The intensity of the peak is substantial and the plane width (101) becomes narrow at the value of $2\theta = 25$. The clarity of the peak indicates the strong crystalline character of the samples. The B-TiO_2 anatase phase is evident from the high diffraction peak at about 25.00 [29]. Based on the Debye-Scherrer's formula, Eq. (2), [30] the average crystalline sizes were 34.2 and 40.2 nm, respectively, for the commercial and B-TiO_2.

$$D = \frac{K\lambda}{\beta\cos\theta} \tag{2}$$

where D refers to the crystallite size, Scherrer constant ($K = 0.94$), wavelength ($\lambda = 0.15418$ nm), β indicates the full width at half maximum (FWHM) of the diffraction peak to the corresponding crystallographic plane of anatase, and θ represents the x-ray diffraction peak angle.

3.2. Photocatalytic activity of B-TiO_2

3.2.1. Different degradation techniques

AMOX removal percentages from aqueous solution were compared by using various techniques of AOPs (solar irradiation/B-TiO_2, solar irradiation/H_2O_2, and solar

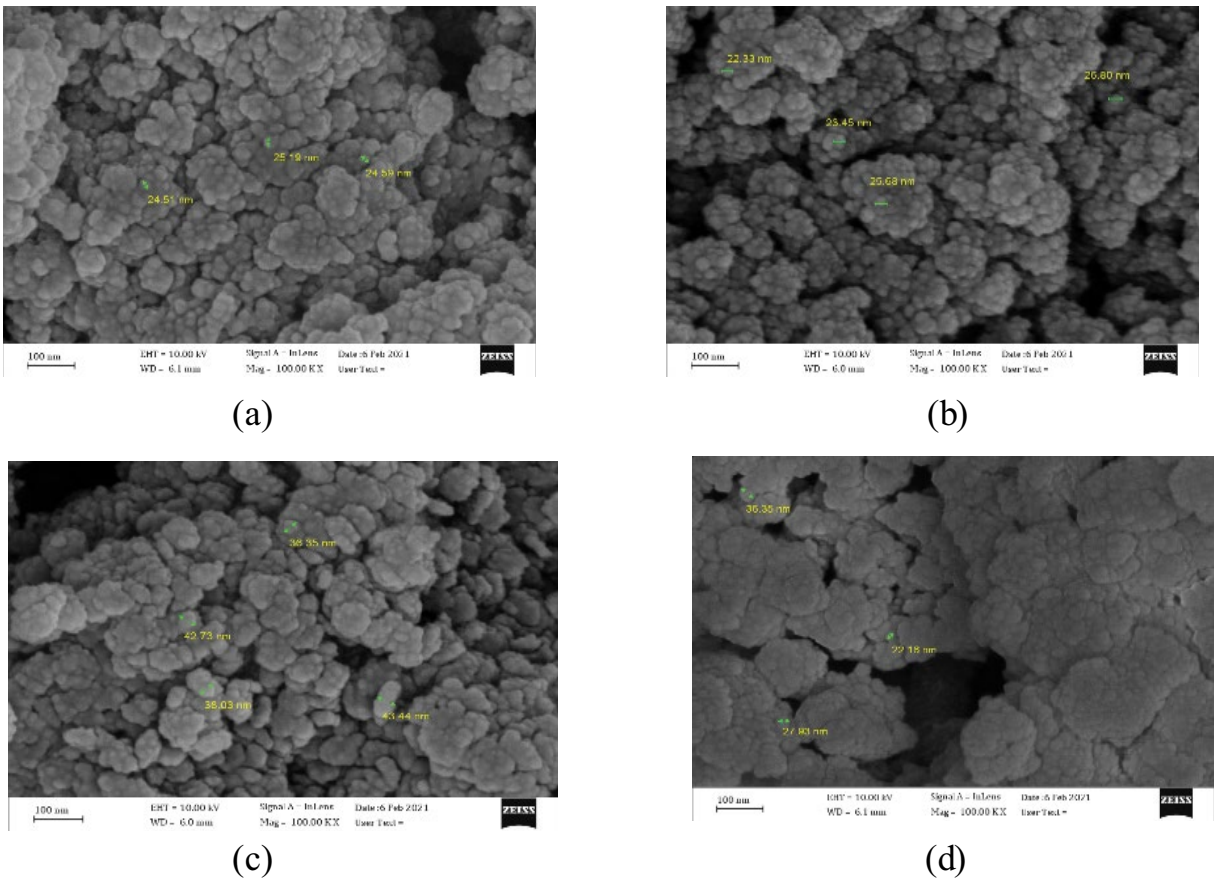

Fig. 3. SEM analysis: (a) commercial TiO_2 before use, (b) B-TiO_2 before use, (c) commercial TiO_2 after use and (d) B-TiO_2 after use.

irradiation/TiO_2/B-H_2O_2 under different operation conditions; 10 mg/L initial AMOX concentration, pH = 7, 25 mg/L B-TiO_2 loadings, and 400 mg/L as initial H_2O_2 concentration at room temperature and their results are plotted in Fig. 5, the results indicate that only 31.25% removal percentage was reached by using solar irradiation/B-TiO_2. while the removal percentage was 58% by the addition of H_2O_2 to solar irradiation. This result was similar to the results reported by [31]. The uses of H_2O_2 in addition to B-TiO_2 in solar irradiation systems faster the degradation rate of AMOX and higher the mineralization level to 84%. It could be mainly due to active kinds produced during the photocatalytic process such as hydroxyl radical.

3.2.2. pH

The pH was found to greatly influence the formation of the hydroxyl radicals, and thus affect the oxidation efficacy. Therefore, experiments were performed to identify the ideal pH by changing the values of the initial pH 3, 5, 7, and 10, but maintaining the other parameters as constant H_2O_2 = 500 mg/L, AMOX conc. = 10 mg/L, time = 150 min, agitation speed = 200 rpm, B-TiO_2 = 25 mg/L (as shown in Fig. 6.) The findings indicate that an increase in the pH value from 3 to 5 caused the removal efficiency to escalate. However, any increase exceeding 5 induced a reduction in the removal efficiency. The reason for the increase in the antibiotic breakdown at an acidic pH was likely due to both antibiotic hydrolysis and H_2O_2 decomposition, occurring at alkaline pH [32].

The poor efficiency observed at an alkaline pH is attributed possibly to the negative charges carried by the AMOX and B-TiO_2, and to the dissociation and autodecomposition of the H_2O_2, whereas the lowered degree of degradation at pH below 5 can be linked to the hydroxyl radical scavenging of the H^+ [33].

In this direction, the analysis of pH_{pzc} is very important to indicate the pH value at which the surface of catalysts is being neutral charge. In other words, the surface charge of the catalysts is negative when the pH values are higher than pH_{pzc} and vice versa [34]. The following equations show that the photocatalyst surface ionization state can be protonated and deprotonated in acidic and alkaline conditions, respectively.

$$pH < PZC \quad TiOH + H^+ \rightarrow TiOH_2^+ \tag{3}$$

$$pH > pzc \quad TiOH + OH^- \rightarrow TiO^- + H_2O \tag{4}$$

The point of zero charges (pzc) of the commercial TiO_2 and B-TiO_2 is vastly studied and their value was pH 6.9 and 7.5, respectively.

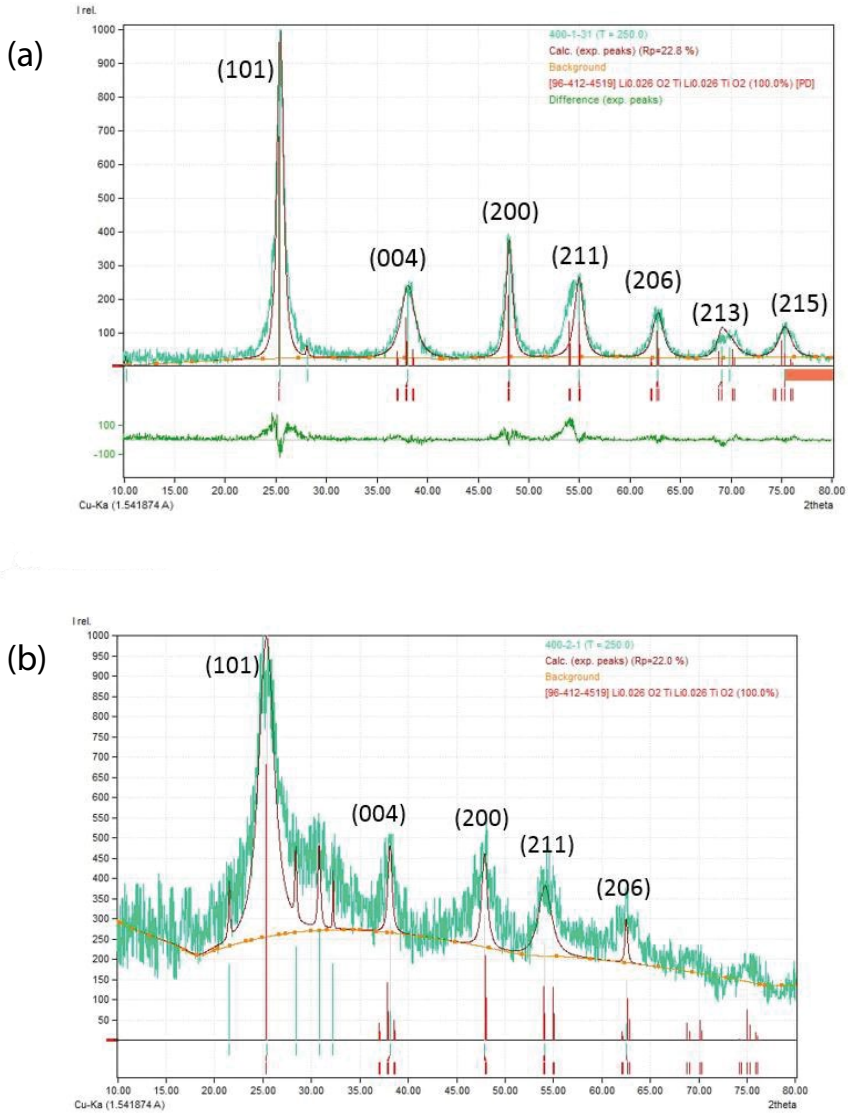

Fig. 4. XRD pattern: (a) commercial TiO_2 and (b) B-TiO_2.

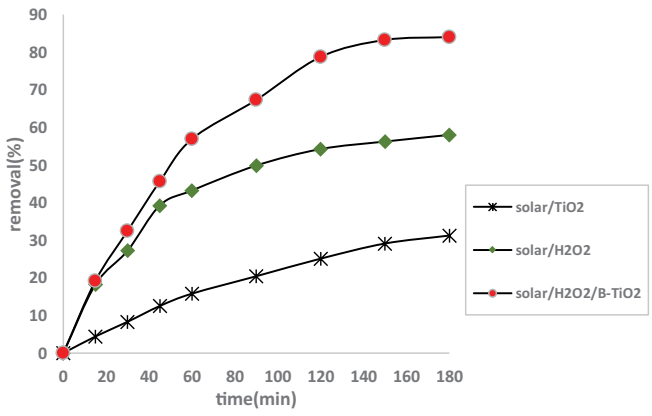

Fig. 5. Degradation of AMOX as a function of different oxidation systems using solar irradiation.

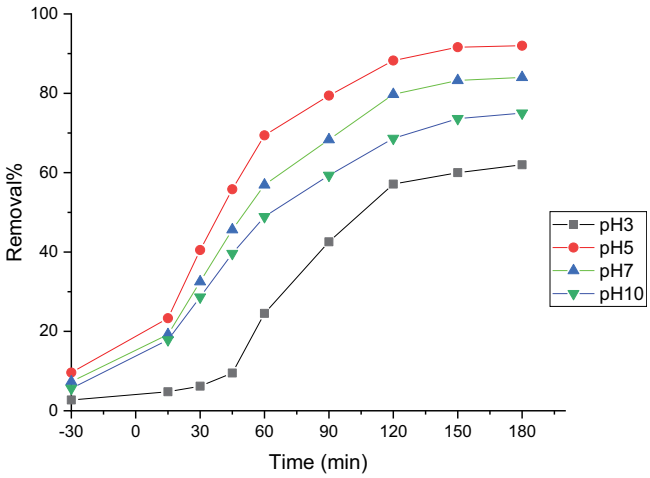

Fig. 6. Influence of pH on AMOX removal by photocatalytic system.

Moreover, the positive holes are considered as the major oxidation species at this pH which react with hydroxide ions forming hydroxyl radicals, thus the efficiency of the process is enhanced. While at pH > 5, there is a columbic repulsion between the negatively charged surface of catalyst and the hydroxide anions, Eq. (4) which prevent the formation of $OH^{\bullet}$ and decrease the photocatalytic degradation. This result was similar to the finding of [35]. The maximum removal efficiency achieved was 91.63% when the pH value was 5, the ideal value of pH 5 was selected, and the remainder of the experiment was performed at this pH.

3.2.3. Initial AMOX concentration

It is very clear from Fig. 7 that the different initial antibiotic concentrations used the removal profile of the AMOX to be in the 10–100 mg/L range, while the other parameters were maintained at constant (H_2O_2 = 500 mg/L, time = 150 min, agitation speed = 200 rpm, B-TiO_2 of 25 mg/L and pH = 5). The findings reveal that when the initial concentration was increased the AMOX degradation percentage declined, attributed to the few numbers of sites available on the molecular surfaces of the catalyst in solution [36,37]. Besides, this figure also reveals that for the reaction time of 150 min, the AMOX degradation spiked in response to an increase in the contact time until 150 min was reached; no significant increase was observed in the removal percentage in response to a further increase in the contact time; this was because the concentrations of the AMOX and H_2O_2 was low. These findings concur with those of Türkay and Kumbur [38].

3.2.4. H_2O_2 concentration

As evident from Eqs. (5) and (6), the hydrogen peroxide concentration plays a critical part in antibiotic degradation because it generates hydroxyl radicals. From Fig. 8 the variations in the AMOX removal are highlighted at different concentrations of H_2O_2 250, 500, and 750 mg/L, while the other parameters are maintained as constant (AMOX concentration of 10 mg/L, B-TiO_2 concentration of 25 mg/L, 150 min, 200 rpm of agitation speed, and pH 5). The results clearly showed that the AMOX removal percentage began to rise in response to the increase in the H_2O_2 concentration until it touched 500 mg/L. However, any further increase in the quantity of the H_2O_2 induced a drop in the degradation efficiency of the AMOX, induced by the auto-decomposition of the H_2O_2 to oxygen and water, as well as by the scavenging of the $OH^{\bullet}$ done by the H_2O_2 [39,40]. The percentage of the AMOX degradation was recorded as 82.35, 91.63, and 74.25 at the concentrations of the H_2O_2 of 250, 500, and 750 mg/L, respectively.

$$2H_2O_2 \rightarrow 2H_2O + O_2 \quad (5)$$

$$OH^{\bullet} + H_2O_2 \rightarrow H_2O + HO_2^{\bullet} \quad (6)$$

3.5. Catalyst concentration and type

The effect of the different doses of B-TiO_2 (25–150) mg/L on the degree of AMOX degradation are presented in Fig. 9; in fact, the results reveal that the removal efficiency decreased from 91.63 to 73.69% when the B-TiO_2 load was increased from 25 to 150 mg/L, respectively. This reduction is ascribed to (i) the creation of aggregates and the catalyst particles undergoing self-binding; at high concentrations, this caused a drop in the number of catalyst reactive sites to decrease; (ii) the reduced light scattering and fewer number of photons, which slowed down the photocatalytic reaction rate; and (iii) the scavenging effect of the percentage of the OH on oxygen removal [41]. The steps cited below can be followed to ascertain the manner in which the TiO_2 is activated by the UV light [26].

$$TiO_2 + h\nu \rightarrow e^- + h^+ \quad (7)$$

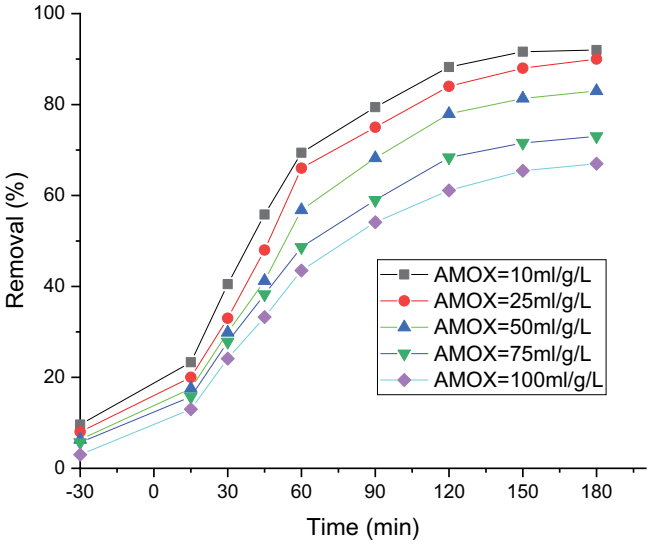

Fig. 7. Influence of amoxicillin concentration on removal by photocatalytic system.

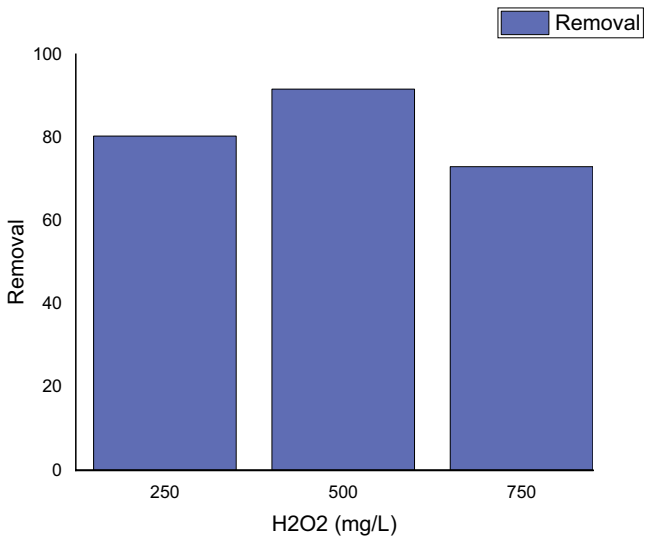

Fig. 8. Influence of H_2O_2 concentration on removal of antibiotic.

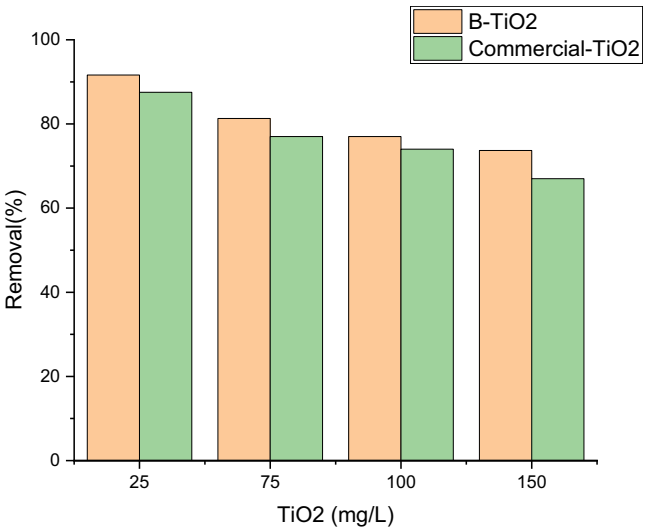

Fig. 9. Influence of catalyst loading on AMOX removal.

$$H^+ + H_2O \rightarrow OH^\bullet + H^+ \quad (8)$$

$$h^+ + OH^- \rightarrow OH^\bullet \quad (9)$$

$$OH^\bullet + \text{AMOX} \rightarrow \text{Degradation products} \quad (10)$$

$$h^+ + \text{AMOX} \rightarrow \text{Oxidation AMOX} \quad (11)$$

$$e^- + O_2 \rightarrow O_2^{-\bullet} \quad (12)$$

$$O_2^{-\bullet} + \text{AMOX} \rightarrow \text{Degradation products} \quad (13)$$

From this figure it is also clear that at constant parameters, when B-TiO_2 is used, the removal efficiency of the AMOX residue is greater than when the commercial TiO_2 is utilized, at 25 mg/L of B-TiO_2 and TiO_2; for 25 mg/L, the removal efficiency showed an increment ratio of more than 4%.

3.6. Total organic carbon removal by AOPs

The total organic carbon (TOC) is measured in pure water and aqueous systems as the whole quantity of carbon present in the organic compounds. Through periodic TOC analyses, the antibiotic degradation was carefully monitored [42]. As it is almost impossible to identify and quantify the innumerable organic molecules available in the wastewaters, it renders the sum-parameter assessment of overall organic carbon more than a simple shortcut to determine the total quantity of organic substances present in a sample. In the present study, the organic carbon present in the AMOX was oxidized to carbon dioxide through a process of chemical oxidation, employing hydroxyl radicals and a catalyst under solar irradiation. The results are shown in Fig. 10. While it is evident the decrease in the TOC concentration occurs as a function of time, this figure also reveals that the hydrogen peroxide used, raises the decomposition of the total organic carbon, by supplying a larger number of hydroxyl radicals [43].

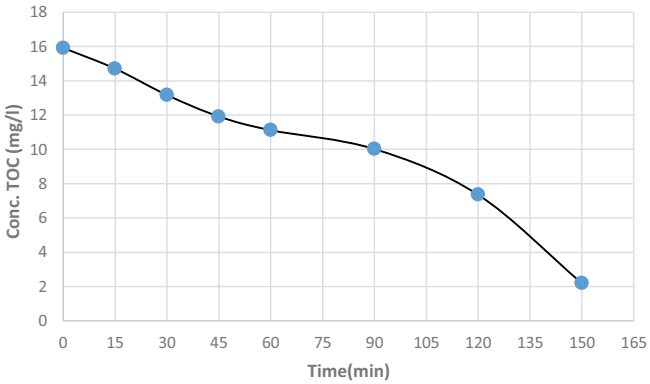

Fig. 10. Shows the decrease in the concentration of total organic carbon.

3.7. Products analysis

As the AMOX structure was broken down, the reaction mixture attained greater complexity induced by the creation of a few small molecular intermediate products. The GC-MS has become a very significant tool used for sample analysis, as it is a combination of both the chromatographic method for efficiently separating the constituents of the sample, and mass spectroscopy, which detects the compounds based on the ratio of their mass to charge (m/z). The chromatogram analyses for the AMOX samples prior to and post the process of degradation under optimum conditions, are shown in Figs. 11 and 12, respectively. Prior to the treatments the high peaks were evident at 17.334 with the following compounds – tridecanoic acid, methyl ester, pentadecanoic acid, 14-methyl, ethyl ester, methyl 11-methyl-dodecanoate; at 19.993 they were observed with the following compounds – octadecenoic acid (Z)-, methyl ester, methyl-11-pentadecen, ol acetate, epoxytetradecan; and at 20.367 the peaks were seen with the compounds cyclopentaneundecanoic acid, methyl ester, heptadecanoic acid, 16-methyl-, ethyl ester and methyl 11-methyl-dodecanoate. After the treatment utilizing B-TiO_2, these peaks were noted to have reduced in intensity, implying that the dissolution of the compounds from toxic to less toxic are indicated by 2-heptenoic acid, methyl ester, succinamic acid, pentanoic acid, 4-methyl-, methyl ester, oxalic acid, allyl hexadecyl ester, allyl undecyl ester, allyl tridecyl ester, hexadecanal, hexadecane, 1-bromo, tetracontane, 3,5,24-trimethyl, 13-octadecenal, 9-octadecenal, (Z)-, 9-methyl-Z, Z-10,12-hexadecadien, acetate, cis-9-hexadecenal and tetradecane. The latter are recognized as biological compounds which appeared to behave as insect-repellent compounds, existing within the basil leaves [12]. As the intermediates accumulate, they can restrict any further AMOX oxidation and its degradation intermediates. In fact, their accumulation may be induced by the reduced rate of generation of the $OH^\bullet$ radicals, as well as to the terminal reaction of the $OH^\bullet$ radicals in a heterogeneous system. Finally, the reactive oxygen species will

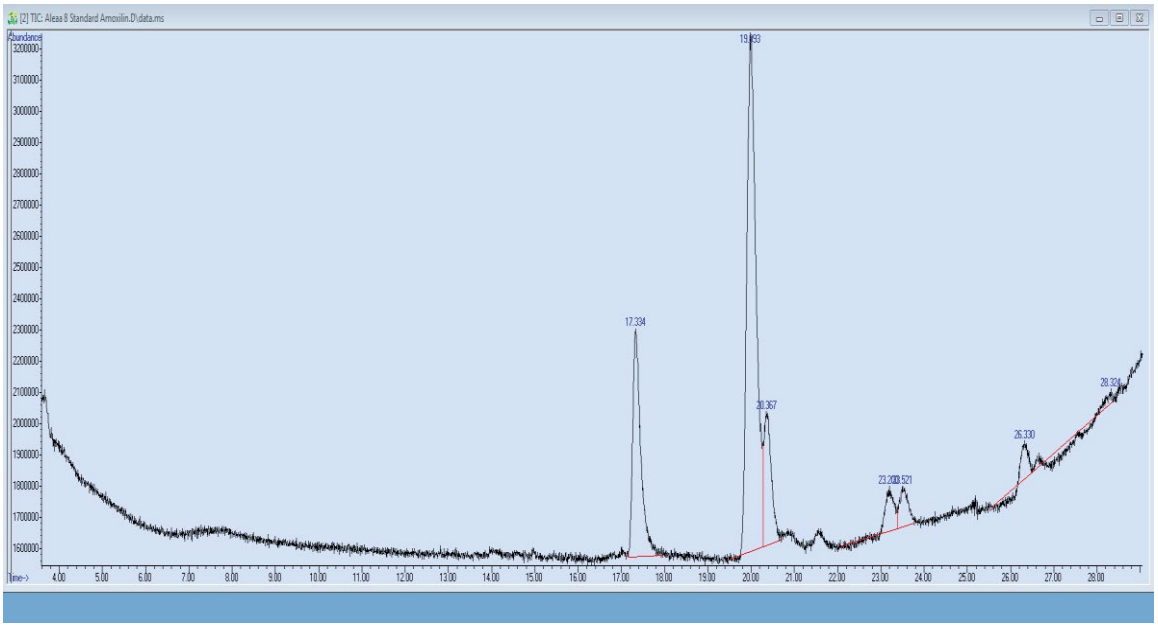

Fig. 11. Mineralization of AMOX during heterogeneous.

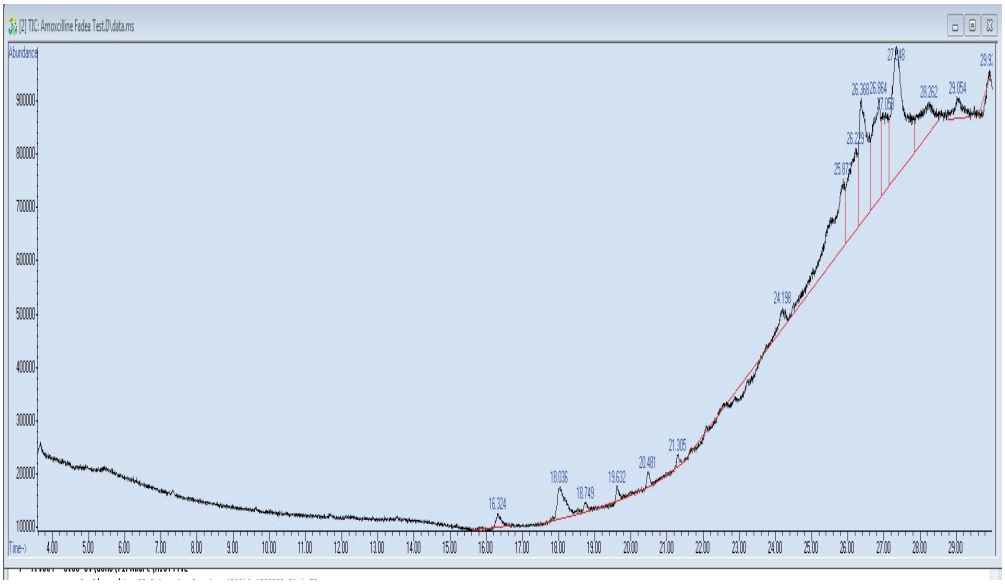

Fig. 12. Chromatogram of AMOX aqueous solution after treatment.

attack all the intermediates cited above even more actively, and transform them into tinier molecules or transform them to carbon dioxide as shown in Eq. (14) [44].

$$\text{Amoxicillin} + {}^{\bullet}\text{OH} \rightarrow \text{Intermediates}$$
$$+ {}^{\bullet}\text{OH} / \text{OH}^{-} / \text{O}^{-2} \rightarrow \text{CO}_2 + \text{H}_2\text{O}$$
$$+ \text{other simpler Z molecules} \quad (14)$$

In the initial molecule breakdown, the lactam group survives and it is off this pathway that the hydroxylation of the aromatic cycle commences. However, during the mass transfer-controlled reaction, the number of different reaction pathways increases because the molecules of the AMOX compete for the active sites present on the surface; the steric obstacles from the AMOX molecules induce the adsorption by several functional groups causing the heterogeneous reaction products and pathways to exhibit higher diversity [45].

4. Conclusion

The green synthesis TiO_2 nanoparticles from the extract of basil leaves (denoted as B-TiO_2) were proved their efficiency in the photocatalytic process for the removal of the

AMOX residue from aqueous solutions, in batch mode reactor using solar irradiation. The success of synthesizing the B-TiO_2 was confirmed through the analyses of the SEM, XRD, and FTIR findings. A variety of parameters were tested, such as the pH, AMOX concentration, and irradiation time, as well as the concentrations of catalyst (B-TiO_2 or TiO_2) and H_2O_2. In conclusion, this study revealed 91.63% and 87.54% was the maximum removal efficiency achieved, respectively at 5 pH, and concentration of 10 mg/L B-TiO_2, 150 min, 25 mg/L, and 500 mg/L H_2O_2, respectively. Besides, from this study, it is clear that 86.24% was the maximum TOC removal achieved. The green synthesis TiO_2 nanoparticles displayed appealing photocatalytic efficiency in the degradation of AMOX residues from aqueous solutions. The findings confirmed the efficacy of the B-TiO_2 as a catalytic in the solar photocatalysis process for removing AMOX from an aqueous solution. However, there are limitations to using suspended photocatalyst in industrial or commercial applications including aggregation during operation, collection after treatment, and reuse. These limitations necessitate additional research for the development of a more easily deployable photocatalyst for such applications.

Acknowledgments

The authors express their gratitude to the University of Baghdad (Baghdad, Iraq) for providing facilities for this research.

References

[1] J. Wang, L. Svoboda, Z. Němečková, M. Sgarzi, J. Henych, N. Licciardello, G. Cuniberti, Enhanced visible-light photodegradation of fluoroquinolone-based antibiotics and *E. coli* growth inhibition using Ag–TiO_2 nanoparticles, RSC Adv., 11 (2021) 13980–13991.
[2] F. Moosavi, C. Cheng, T.T. Gheinani, M. Traore, A. Kanaev, M. Nikravech, Photocatalytic destruction of amoxicillin in a pilot sunlight reactor with supported titania nano-photocatalyst, Chem. Eng. Trans., 73 (2019) 175–180.
[3] S. Saeid, P. Tolvanen, N. Kumar, K. Eränen, J. Peltonen, M. Peurla, J.-P. Mikkola, A. Franz, T. Salmi, Advanced oxidation process for the removal of ibuprofen from aqueous solution: a non-catalytic and catalytic ozonation study in a semi-batch reactor, Appl. Catal., B, 230 (2018) 77–90.
[4] S.J. Olusegun, G. Larrea, M. Osial, K. Jackowska, P. Krysinski, Photocatalytic degradation of antibiotics by superparamagnetic iron oxide nanoparticles. Tetracycline case, Catalysts, 11 (2021) 1243, doi: 10.3390/catal11101243.
[5] E.M. Cuerda-Correa, M.F. Alexandre-Franco, C. Fernández-González, Advanced oxidation processes for the removal of antibiotics from water. An overview, Water, 12 (2020) 102, doi: 10.3390/w12010102.
[6] N.A. Mohammed, A.I. Alwared, M.S. Salman, Photocatalytic degradation of reactive yellow dye in wastewater using H_2O_2/TiO_2/UV technique, Iraqi J. Chem. Petrol. Eng., 21 (2020) 15–21.
[7] B.A. Marinho, L. Suhadolnik, B. Likozar, M. Huš, Z. Marinko, M. Čeh, Photocatalytic, electrocatalytic and photoelectrocatalytic degradation of pharmaceuticals in aqueous media: analytical methods, mechanisms, simulations, catalysts and reactors, J. Cleaner Prod., 343 (2022) 131061, doi: 10.1016/j.jclepro.2022.131061.
[8] H.A. Patehkhor, M. Fattahi, M. Khosravi-Nikou, Synthesis and characterization of ternary chitosan–TiO_2–ZnO over graphene for photocatalytic degradation of tetracycline from pharmaceutical wastewater, Sci. Rep., 11 (2021) 24177, doi: 10.1038/s41598-021-03492-5.
[9] H. Mahmoodi, M. Fattahi, M. Motevassel, Graphene oxide–chitosan hydrogel for adsorptive removal of diclofenac from aqueous solution: preparation, characterization, kinetic and thermodynamic modelling, RSC Adv., 11 (2021) 36289–36304.
[10] A. Garmroudi, M. Kheirollahi, S.A. Mousavi, M. Fattahi, E.H. Mahvelati, Effects of graphene oxide/TiO_2 nanocomposite, graphene oxide nanosheets and Cedr extraction solution on IFT reduction and ultimate oil recovery from a carbonate rock, Petroleum, (2022), doi: 10.1016/j.petlm.2020.10.002 (in Press).
[11] R.D.H. Abdul Jalill, R.S. Nuaman, A.N. Abd, Biological synthesis of titanium dioxide nanoparticles by *Curcuma longa* plant extract and study its biological properties, World Scientific News, 49 (2016) 204–222.
[12] P. Kantheti, P. Alapati, Green synthesis of TiO_2 nanoparticles using *Ocimum basilicum* extract and its characterization, Int. J. Chem. Stud., 6 (2018) 670–674.
[13] T.B. Alobaidi, A.I. Alwared, Biosynthetic of titanium dioxide nanoparticles using *Zizyphus spina-christi* leaves extract: properties, J. Ecol. Eng., 23 (2022) 315–324.
[14] T. Pushpamalini, M. Keerthana, R. Sangavi, A. Nagaraj, P. Kamaraj, Comparative analysis of green synthesis of TiO_2 nanoparticles using four different leaf extract, Mater. Today: Proc., 40 (2021) S180–S184.
[15] V. Patidar, P. Jain, Green synthesis of TiO_2 nanoparticle using *Moringa oleifera* leaf extract, Int. Res. J. Eng. Technol., 4 (2017) 470–473.
[16] R.K. Ganapathi, C.H. Ashok, R.K. Venkateswara, C.H. Chakra, P. Tambur, Green synthesis of TiO_2 nanoparticles using *Aloe vera* extract, J. Res. Phys. Sci. (IJARPS), 2 (2015) 28–34.
[17] R. Sankar, K. Rizwana, K.S. Shivashangari, V. Ravikumar, Ultrarapid photocatalytic activity of *Azadirachta indica* engineered colloidal titanium dioxide nanoparticles, Appl. Nanosci., 5 (2015) 731–736.
[18] K. Velayutham, A.A. Rahuman, G. Rajakumar, T. Santhoshkumar, S. Marimuthu, C. Jayaseelan, A. Bagavan, A.V. Kirthi, C. Kamaraj, A.A. Zahir, G. Elango, Evaluation of *Catharanthus roseus* leaf extract-mediated biosynthesis of titanium dioxide nanoparticles against *Hippobosca maculata* and *Bovicola ovis*, J. Parasitol. Res., 111 (2012) 2329–2337.
[19] M. Sundrarajan, S. Gowri, Green synthesis of titanium dioxide nanoparticles by Nyctanthes Arbor-Tristis leaves extract, Chalcogenide Lett., 8 (2011) 447–451.
[20] S. Ye, Y. Chen, X. Yao, J. Zhang, Simultaneous removal of organic pollutants and heavy metals in wastewater by photoelectrocatalysis: a review, Chemosphere, 273 (2021) 128503, doi: 10.1016/j.chemosphere.2020.128503.
[21] D. Balarak, F.K. Mostafapour, A. Joghtaei, Thermodynamic analysis for adsorption of amoxicillin onto magnetic carbon nanotubes, J. Pharm. Res. Int., 16 (2017) 1–11, doi: 10.9734/BJPR/2017/33212.
[22] M. Zaier, L. Vidal, S. Hajjar-Garreau, L. Balan, Generating highly reflective and conductive metal layers through a light-assisted synthesis and assembling of silver nanoparticles in a polymer matrix. Sci. Rep., 7 (2017) 12410, doi: 10.1038/s41598-017-12617-8.
[23] E. Bazrafshan, T.J. Al-Musawi, M.F. Silva, A.H. Panahi, M. Havangi, F.K. Mostafapur, Photocatalytic degradation of catechol using ZnO nanoparticles as catalyst: optimizing the experimental parameters using the Box–Behnken statistical methodology and kinetic studies, Microchem. J., 147 (2019) 643–653.
[24] A.A. Mohammed, T.J. Al-Musawi, S.L. Kareem, M. Zarrabi, A.M. Al-Ma'abreh, Simultaneous adsorption of tetracycline, amoxicillin, and ciprofloxacin by pistachio shell powder coated with zinc oxide nanoparticles, Arabian J. Chem., 13 (2020) 4629–4643.
[25] A. Chatterjee, D. Nishanthini, N. Sandhiya, J. Abraham, Biosynthesis of titanium dioxide nanoparticles using *Vigna radiate*, Asian J. Pharm. Clin. Res., 9 (2016) 85–88.
[26] M. Malakootian, A. Nasiri, M.A. Gharaghani, Photocatalytic degradation of ciprofloxacin antibiotic by TiO_2 nanoparticles immobilized on a glass plate, Chem. Eng. Commun., 207 (2020) 56–72.

[27] F.I. Al Qarni, N.A. Alomair, H.H. Mohamed, Environment-friendly nanoporous titanium dioxide with enhanced photocatalytic activity, Catalysts, 9 (2019) 799, doi: 10.3390/catal9100799.
[28] X. Wei, G. Zhu, J. Fang, J. Chen, Synthesis, characterization, and photocatalysis of well-dispersible phase-pure anatase TiO_2 nanoparticles, J. Photoenergy, 2013 (2013) 726872, doi: 10.1155/2013/726872.
[29] M.I. Pratheepa, M. Lawrence, X-ray diffraction analyses of titanium dioxide nanoparticles, Int. J. Sci. Res. Sci. Technol. (IJSRST), 3 (2017) 83–88.
[30] J.S.J. Hargreaves, Some considerations related to the use of the Scherrer equation in powder X-ray diffraction as applied to heterogeneous catalysts, Catal. Struct. React., 2 (2016) 33–37.
[31] I. Kim, N. Yamashita, H. Tanaka, Performance of UV and UV/H_2O_2 processes for the removal of pharmaceuticals detected in secondary effluent of a sewage treatment plant in Japan, J. Hazard. Mater., 166 (2009) 1134–1140.
[32] E.S. Elmolla, M. Chaudhuri, Photocatalytic degradation of amoxicillin, ampicillin and cloxacillin antibiotics in aqueous solution using UV/TiO_2 and UV/H_2O_2/TiO_2 photocatalysis, Desalination, 252 (2010) 46–52.
[33] M. Tamimi, S. Qourzal, N. Barka, A. Assabbane, Y. Ait-Ichou, Methomyl degradation in aqueous solutions by Fenton's reagent and the photo-Fenton system, Sep. Purif. Technol., 61 (2008) 103–108.
[34] Y. Sun, Q. Yue, B. Gao, B. Wang, Q. Li, L. Huang, X. Xu, Comparison of activated carbons from *Arundo donax Linn* with $H_4P_2O_7$ activation by conventional and microwave heating methods, Chem. Eng. J., 192 (2012) 308–314.
[35] S. Alahiane, S. Qourza, M. El Ouardi, A. Abaamrane, A. Assabbane, Factors influencing the photocatalytic degradation of Reactive yellow 145 by TiO_2-coated non-woven fibers, Am. J. Anal. Chem., 5 (2014) 445–454.
[36] A. Nikravan, Amoxicillin and Ampicillin Removal From Wastewater by Fenton and Photo-Fenton Processes, Hacettepe University, 2015, p. 122.
[37] F.-S. Tabatabai-Yazdi, P.A. Ebrahimian, K.F. Esmaeili, K.N. Asasian, N. Gilani, Photocatalytic treatment of tetracycline antibiotic wastewater by silver/TiO_2 nano sheets/reduced graphene oxide and artificial neural network modeling, Water Environ. Res., 92 (2020) 662–676.
[38] G.K. Türkay, H. Kumbur, Investigation of amoxicillin removal from aqueous solution by Fenton and photocatalytic oxidation processes, Kuwait J. Sci., 46 (2019) 85–93
[39] E. Elmolla, M. Chaudhuri, Optimization of Fenton process for treatment of amoxicillin, ampicillin and cloxacillin antibiotics in aqueous solution, J. Hazard. Mater., 170 (2009) 666–672.
[40] G.V. Buxton, C.L. Greenstock, W. Phillips Helman, A.B. Ross, Critical review of rate constants for reactions of hydrated electrons, hydrogen atoms and hydroxyl radicals ($^{\bullet}OH/^{\bullet}O^-$) in aqueous solution, J. Phys. Chem. Ref. Data, 17 (2011), doi: 10.1063/1.555805.
[41] B. Kakavandi, N. Bahari, R. Rezaei Kalantary, F.E. Dehghani, Enhanced sono-photocatalysis of tetracycline antibiotic using TiO_2 decorated on magnetic activated carbon (MAC@T) coupled with US and UV: a new hybrid system, Ultrason. Sonochem., 55 (2019) 75–85.
[42] R.B.P. Marcelino, L.N. Andrade, M.C.V.M. Starling, C.C. Amorim, M.L.T. Barbosa, R.P. Lopes, B.G. Reis, M.M.D. Leão, Evaluation of aerobic and anaerobic of real pharmaceutical wastewater from industrial production of antibiotics, Braz. J. Chem. Eng., 33 (2016) 445–452.
[43] S. Loaiza-Ambuludi, M. Panizza, N. Oturan, M.A. Oturan, Removal of the anti-inflammatory drug ibuprofen from water using homogeneous photocatalysis, Catal. Today, 224 (2014) 29–33.
[44] N. Olama, M. Dehghani, M. Malakootian, The removal of amoxicillin from aquatic solutions using the TiO_2/UV-C nanophotocatalytic method doped with trivalent iron, Appl. Water Sci., 8 (2018) 1–12, doi: 10.1007/s13201-018-0733-7.
[45] D. Klauson, J. Babkina, K. Stepanova, M. Krichevskaya, S. Preis, Aqueous photocatalytic oxidation of amoxicillin, Catal. Today, 151 (2010) 39–45.